1-1-2013

Roles of compressive residual stress in enhancing the corrosion resistance of nano nitride composite coatings on steel

Xiaoli Zhao
Edith Cowan University

Paul Munroe

Daryoush Habibi
Edith Cowan University

Zonghan Xie
Edith Cowan University

10.1016/j.jascer.2013.03.002
Zhao, X. , Munroe, P., Habibi, D. , & Xie, Z. (2013). Roles of compressive residual stress in enhancing the corrosion resistance of nano nitride composite coatings on steel. Journal of Asian Ceramic Societies, 1(1), 86-94. Available here

Journal of Asian Ceramic Societies 1 (2013) 86–94

Journal of Asian Ceramic Societies

Journal of Asian Ceramic Societies

journal homepage: www.elsevier.com/locate/jascer

Roles of compressive residual stress in enhancing the corrosion resistance of nano nitride composite coatings on steel

Xiaoli Zhao[a,*], Paul Munroe[b], Daryoush Habibi[a], Zonghan Xie[c,**]

[a] School of Engineering, Edith Cowan University, Perth, WA 6027, Australia
[b] School of Materials Science and Engineering, University of New South Wales, Sydney, NSW 2052, Australia
[c] School of Mechanical Engineering, University of Adelaide, Adelaide, SA 5005, Australia

ARTICLE INFO

Article history:
Received 16 January 2013
Received in revised form 5 March 2013
Accepted 5 March 2013
Available online 9 April 2013

Keywords:
Ceramic
Stress corrosion
Sputtered films
SEM
Modeling studies

ABSTRACT

Nanocomposite coatings were synthesized, and subsequently annealed, in an attempt to understand the influence of residual stress upon their resistance to corrosion under acidic attack. Pitting corrosion, originating from microscopic coating defects, was commonly identified in the coatings subject to annealing. Finite element analysis was used to map the residual stress distribution adjacent to these defects and quantify resulting geometrical changes. The results show that with the presence of compressive residual stress in the coatings, corrosion-initiated cracking along weak interfaces was suppressed, and structural integrity maintained. Moreover, compressive residual stress helped constrict pre-existing structural defects in columnar-structured coatings and, in doing so, block the pathway of corrosive agents and limit corrosion damage to the coating–substrate interface and the substrate. The closure aspect ratio of the coating defects, defined as a new key indicator to the corrosion resistance, was numerically evaluated and quantitatively discussed for TiN coatings. Coating corrosion resistance may be improved by optimizing the residual stress in conjunction with coating thickness and the geometry of common defects.

1. Introduction

Corrosion is ubiquitous and the corrosion of steel-based components is estimated to cost about 3% of world gross domestic product every year [1]. To combat corrosion, advanced ceramic coatings prepared using a range of deposition techniques have attracted considerable attention in recent years [2–4]. Their corrosion behavior has been studied using electron microscopy and a variety of other surface analytical techniques [5–9].

Although corrosion is an electrochemical reaction, the process is also strongly influenced by the mechanical and microstructural properties of the material being investigated. In addition to the chemical composition of the coating layer, the corrosion resistance of ceramic coated steels is also affected by a number of physical and structural factors. For example, ceramic coatings prepared by physical vapor deposition (PVD) often possess microscopic defects, such as pinholes or embedded particles [10,11]. These structural defects may act as pathways for corrosive agents to penetrate through the coating barrier and initiate localized corrosion in the less-noble metal substrate [12,13]. Stress corrosion cracking (SCC) is frequently used to describe the premature failure of metals when subjected to tensile stress in a corrosive environment [14–17]. On the other hand, compressive stress has been found to help inhibit the corrosion of materials [18]; however, the underlying mechanism of such an inhibiting effect remains largely unknown. Significantly, compressive residual stresses often exist in ceramic coatings deposited by PVD on steel substrates [19,20]. Various methods have been proposed to quantify and control the stress level [21–24], in order to improve the mechanical performance of as-deposited coatings [25,26].

Recently, a nanocomposite multilayer coating was synthesized to protect metallic components used in high speed machining and medical devices. Focused ion beam (FIB) microscopy revealed that this novel coating consists of a superhard nanocomposite TiSiN

* Corresponding author at: School of Engineering, Edith Cowan University, 270 Joondalup Drive, Joondalup, WA 6027, Australia. Tel.: +61 8 6304 5782; fax: +61 8 6304 5811.
** Corresponding author. Tel.: +61 8 8313 3980; fax: +61 8 8313 4367.
E-mail addresses: x.zhao@ecu.edu.au (X. Zhao), zonghan.xie@adelaide.edu.au (Z. Xie).

Peer review under responsibility of The Ceramic Society of Japan and the Korean Ceramic Society.

Production and hosting by Elsevier

2187-0764 © 2013 The Ceramic Society of Japan and the Korean Ceramic Society. Production and hosting by Elsevier B.V. All rights reserved.
http://dx.doi.org/10.1016/j.jascer.2013.03.002

outer layer, a tough columnar-structured TiN inner layer and a Ti wetting layer [27,28]. Moreover, a thermal annealing treatment was found to be effective in reducing the residual stress in the coating without altering its microstructure [29]. It was also identified, with the help of finite element analysis (FEA), that the propagation of corrosion through the coating layers was suppressed by compressive residual stress which causes the shrinkage of open corrosion paths in the coatings [30]. However, the modeling and analysis in [30] showed that the compressive stress resulted in only limited reduction in the cross-sectional area of corrosion pits. Therefore, this alone cannot explain the marked difference in the corrosion resistance observed experimentally. Also notably, the influence of the compressive stress over pre-existing structural defects, such as pores, pinholes and fissures, has not been taken into account in the aforementioned modeling. Yet, the latter are far more important, for it is much easier and faster for corrosive agents to penetrate a ceramic coating through pre-existing defects, than passing through the coating via corrosion pits resulting from the corrosion process itself.

In this work, the newly developed TiSiN and TiN coating were used as a model system to clarify the critical factors that governed their corrosion resistance. First, the evolution of corrosion during immersion tests and its interaction with the coating microstructure were examined, extended from previous investigations [30]. Then, FEA was applied to simulate the re-distribution of stress within the vicinity of pre-existing defects, with emphasis on how the localized stress modifies the geometry of pre-existing defects, which in turn influences the corrosion resistance of the coating layer. Finally, a direct link between surface defects and residual stress with the corrosion resistance of ceramic coatings was established.

2. Experimental

2.1. Sample preparation

Nanocomposite multilayer coatings were deposited onto AISI M42 tool steel substrates by PVD using a reactive close-field unbalanced magnetron sputtering system (UDP650, Teer Coatings Ltd., Droitwich, Worcestershire, UK). Details of the deposition procedure have been given elsewhere [29] and can be summarized as follows: first, oxides and other contaminants on the substrate surface were removed by Ar ion bombardment. Then, a Ti wetting layer ~0.22 μm in thickness was deposited, followed by a TiN transitional layer of ~1 μm in thickness. Finally, a TiSiN coating layer ~1.78 μm in thickness was deposited. This was composed of ~50 at.% of Ti, ~10 at.% of Si and ~40 at.% of N, as determined by X-ray photoelectron spectroscopy (XPS). After deposition, some of the samples were annealed for 3 h in a Carbolite vacuum tube furnace at 900 °C with a base pressure $<1 \times 10^{-6}$ Torr and a heating and cooling rate of 5 °C/min. The residual stress in the TiSiN coatings was found to decrease from ~10 GPa to ~1 GPa after thermal annealing, according to a recent nanoindentation study [29].

2.2. Corrosion tests

The samples for immersion tests were coated by protective lacquer to expose only the coated area. The test was performed in a 70% HNO_3 solution at 25 °C. The immersion period was set to either 2 or 8 days. Five samples for each coating condition, including the as-deposited, and samples subjected to either 2 or 8 days immersion, were prepared and tested.

2.3. Surface and subsurface observation

The surface of both reference and corroded samples was examined using a field emission scanning electron microscope (FESEM) (Model Fei Nova 230, FEI Company, Hillsboro, OR, USA). Sectioning and imaging of the corrosion damage in the annealed sample was conducted using a Neon 40EsB (Zeiss, Oberkochen, Germany) focused ion beam scanning electron microscope (FIB-SEM). Sectioning of the subsurface was achieved using the FIB to expose a cross-section of the sample. Images were collected using an in-lens secondary electron detector. Sectioning and subsurface imaging of other samples were carried out using a FIB workstation (FEI xP200 focused ion beam microscope, FEI Company, Hillsboro, OR, USA). The procedure has been described elsewhere [27]. First, a high gallium ion beam current (~7000 pA) was used to mill through the surface area of interest and create a wedge-like trench. The resultant rough cross-section was then polished at medium currents (1000–3000 pA) to remove particle deposition and smooth the surface. Finally, the cross-section was imaged at lower beam currents (~70 pA).

2.4. Simulation method

Two types of FEA models were constructed using COMSOL Multiphysics software (Version 3.5a, Burlington, MA 01803, USA) to analyze the distribution of residual stress in the vicinity of pre-existing coating defects, such as a micro-sized pores (typically > 5 μm in diameter), a nano-sized pinhole (typically ~30 nm in diameter), and a long fissure (typically ~30 nm in width). The first model focused on the micro-sized pore-type defects, from which corrosion cavities were developed in the coating layer. This model was constructed in an axisymmetric fashion (Fig. 1(a) and (b)). The sizes of the cross-section of the defects in the model were estimated from the FIB-generated images, with the diameters of the pores being 5 μm and 8 μm at the top of TiN and TiSiN layers, respectively. The second model dealt with pre-existing nano-scale defects with a typical diameter or width below 100 nm. These defects reside in the TiN layer of 1 μm thickness, which aligned vertically and acted as passages for corrosion agents. Both pin-hole (Fig. 1(c) and (e)) and long fissure type defects (Fig. 1(d) and (e)) were modeled, the former using an axisymmetric model, and the latter using a 2D plane strain symmetric model.

FEA meshes were generated in an interactive manner to ensure that the mesh is denser around the edges, where large stress gradients, even singularities, may arise (Fig. 1(b) and (e)). This was done by specifying the mesh size and the element growth rate at critical locations. Boundary conditions are described below. For the axisymmetric models, the left-hand side was the axial symmetry axis. The bottom and the right-hand side were fixed along the z and r directions, respectively, but were free to move in the other directions. For the 2D plane strain model, the left-hand side represented the symmetric plane, and the bottom and the right-hand sides were fixed along the z and x directions, respectively. For all the models used, the overall dimension of the model was considerably larger than the coating thickness, thus the edge effect due to boundary constrains was negligible.

The physical parameters of the TiSiN, TiN and Ti sublayers in the coatings are given in Table 1. In the modeling process no external load was applied. Residual stress, assumed to be homogeneous in each coating sublayer (Table 1), was the only source that induced the internal stress distribution. The Ti buffer layer was assumed to be stress-free, since both the substrate and the Ti layer have similar thermal expansion coefficients. Compressive planar stresses were assumed to be present in both TiN and TiSiN layers, the origin of which was a combination of both intrinsic and

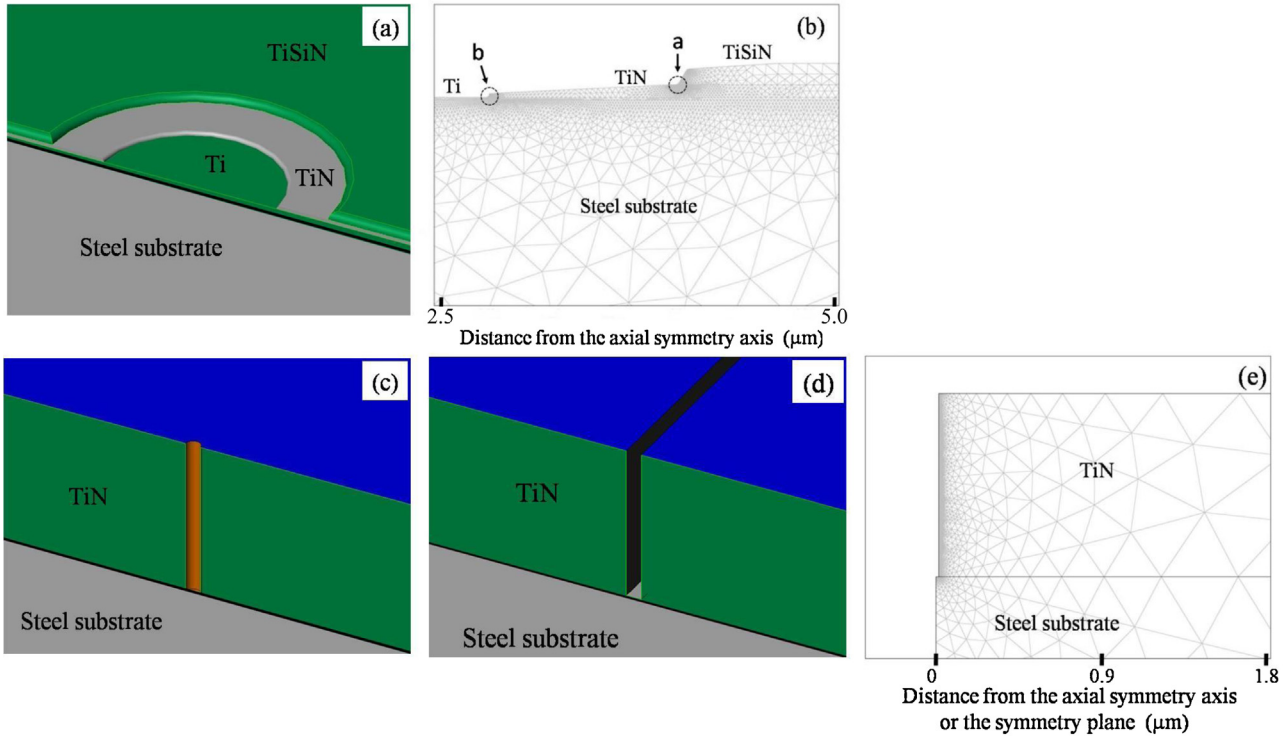

Fig. 1. Finite element models used in mapping the stress distribution around pre-existing structural defects. (a) 3D cross-sectional view of a micron-scale pit, exposing both TiSiN and TiN sublayers, not to scale. (b) Meshes around the cavity in (a), modeled in an axial symmetric fashion; denser meshes are created in the regions *a* and *b*, where stress concentrations may arise. (c) 3D cross-sectional view of a nano-scale hole through the TiN sublayer, not to scale. (d) 3D cross-sectional view of a nanometer wide fissure running through the TiN sublayer, not to scale. (e) Meshes around the structural defects presented in (c) and in (d). Note, although the 2D meshes (i.e., (e)) generated from models (c) and (d) looks identical, in the simulations the former uses an axisymmetric model algorism, while the latter adopts a plane-strain algorism with a 2D plane symmetry.

extrinsic components [19]. For the as-deposited sample, the stresses of TiN and TiSiN sublayers were set to be 3 GPa [31] and 10 GPa [29], respectively. For the annealed sample, these values were reduced to 0.3 GPa and 1 GPa, respectively [29].

3. Results and discussion

3.1. Experimental observation

The nanocomposite outer layer (i.e., TiSiN) showed remarkable integrity and corrosion tolerance in an acidic environment. This was evident from the observation that after the 8 days immersion test the nanocomposite coating, in general, remained intact, except in regions where original surface defects existed (Fig. 2(a) and (b)). These defects, normally having a diameter larger than the coating thickness, were seen in both the as-deposited and annealed samples before the immersion test ([30] and Fig. 2(c)). Pitting originating from these sites was seen in both the as-deposited and annealed samples (Fig. 2(a)).

Table 1
Material properties and thicknesses of the substrate and coating layers used in the FEM simulation.

	Substrate	TiSiN	TiN	Ti
Young's modulus (GPa)	200[a]	510 [29]	590[b]	104[a]
Poisson's ratio	0.30[a]	0.20	0.25	0.34[a]
Residual stress, as-deposited (GPa)	–	10	3	–
Residual stress, annealed (GPa)	–	1	0.3	–
Thickness (μm)	–	1.78	1.00	0.22

Source:
[a] http://www.efunda.com/materials/alloys/.
[b] http://www.ceramics.nist.gov/srd/scd/Z00220.htm.

Subsurface observation of corrosion damage sites, enabled by FIB, was conducted to identify the interaction between the coating microstructure and corrosion progression in the presence of compressive residual stress. After the 2-day immersion tests, the lateral expansion of the pits along the TiSiN/TiN interface was observed in both types of TiSiN coating, since the TiN layer within the pits acted as a physical barrier against downward progression of corrosion. Representative results are shown in Fig. 3(a) and (b), which have been adapted from our previous work [30]. On closer examination, the corrosion agent seemed to penetrate through an intercolumnar fissure within the TiN layer of the annealed sample, forming a corrosion path evident near the bottom of the TiN layer (Fig. 3(b)). In contrast, there was no vertical corrosion penetration in the as-deposited sample (Fig. 3(a)). After the 8-day immersion tests, edge cracks, which appeared along the TiSiN/TiN interface at the corner of the pore, were observed to propagate along the TiSiN/TiN interface, in both the as-deposited and annealed samples (Fig. 3(c) and (d)). However, for the annealed sample the crack was more severe than that in the as-deposited sample. Furthermore, at the interface between the TiN and the steel substrate, delamination occurred only in the annealed sample, even though the TiN layer appeared intact. This may be attributed to the penetration of corrosion agent through small pinholes, as indicated in Fig. 3(b).

Therefore, two different processes that govern pitting were identified here. The first was related to cracks initiating at the corner of pre-existing micron-scale defects which propagated along the interface, while the second was the delamination along the interface between the columnar-structured TiN and the substrate,

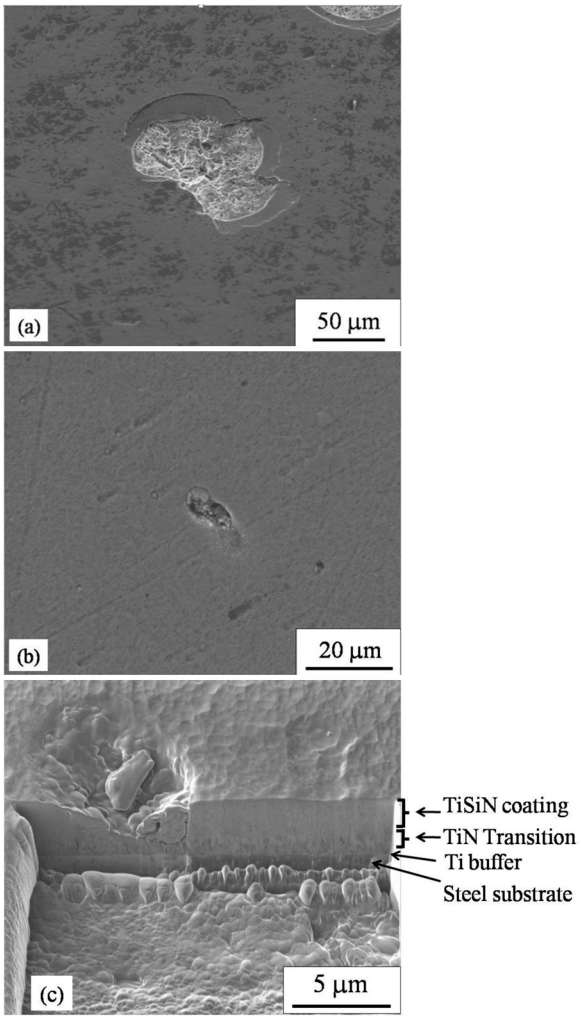

Fig. 2. Observation of micron-scale surface defects and corrosion damage originating from these defects in the samples. (a) Scanning electron microscope image of the surface of the annealed sample after an 8-day immersion test. Note that nanocomposite outer layer shows high corrosion resistance and the pitting is initiated from a surface defect. (b) Scanning electron microscope image of a large pit in the annealed sample before the corrosion test. (c) Focused ion beam (FIB) generated cross-sectional micrograph of a pre-existing pit in the annealed sample before the corrosion test [30]. Note that the defect is confined in the TiSiN layer and neither cracks nor delamination exists around it.

resulting presumably from penetration of corrosion agent through nano-scale pin-holes and features.

3.2. FEA modeling of micro-sized defects

These pre-existing defects normally have a diameter which is larger than the thickness of the coating. As expected, our modeling results indicated that the stress distribution was significantly modified compared to a defect-free coating on the same substrate, particularly at the corner of the pore, where cracks were observed along the interface. The stress distribution pattern observed at region *b* was similar to that at region *a* for both the as-deposited and annealed samples (refer to Fig. 1(b) for regions *a* and *b*), with a lower stress magnitude in the annealed sample. Accordingly, the discussion will be concentrated on region *a*, where edge cracks were experimentally observed.

An in-plane tensile stress is known to have a detrimental effect on the corrosion resistance of metallic components that operate in a corrosive environment [17,32], while, conversely, compressive stresses have been shown to resist corrosion damage [18]. As such, the in-plane compressive stress in the coatings is expected to suppress corrosion in the coated samples. Of significant relevance to the initial corrosion process are the stress components near the surface of the pitting site, which can be best described using a principal axis system. This is because the stress field close to the surface was modified by the defect, as a result, the default axes are no longer parallel with the principal axes. In the case of the as-deposited sample, the residual stress component normal to the surface of a pitting site within the viewing plane, σ_{11}, remained zero at the surface level, due to the relaxation of the stress at the free boundaries (Fig. 4(a)). As such, close to the surface there were only two stress components: (a) the second principal stress, σ_{22}, also called the hoop stress, which was normal to the viewing plane and was compressive in nature (Fig. 4(a) and (b)). The third principal stress σ_{33}, which was within the viewing plane and compressive in nature (Fig. 4(c)), is indicated by the arrows in Fig. 4(a). Distribution of σ_{22} and σ_{33} along the surface of the corrosion cavity were also plotted in Fig. 5(a). These results showed that the original residual stress distribution at the corrosion site changed significantly, compared to regions away from the pitting site where the residual stress was distributed uniformly within the coating layers. The maximum values for σ_{22} and σ_{33} were ~1.5 and ~3 times as large as that of the residual stress within the TiSiN coating layer, respectively, and appeared at the pitting edge. It was noted in a previous study that after annealing at 900 °C, there was no obvious change in the structural and mechanical properties of this coating/substrate system, but the residual stress decreased significantly [29]. Consequently, in both regions *a* and *b* the maximum compressive stress for σ_{22} and σ_{33} in the as-deposited sample was ~9 times larger than those within the annealed sample (Table 2), with the latter being subjected to much more severe corrosion damage as observed from experimental results. This validated the assumption that the compressive stress in the coatings plays a positive role in resisting corrosion development.

Table 2
Maximum stresses (in GPa) in regions *a* and *b* from simulation. The maximum values of σ_{22} and σ_{33} are evaluated along the corrosion cavity surfaces (refer to Fig. 5(a)), while the maximum values of σ_{zz} and σ_{rz} are obtained along the interfaces (refer to Fig. 5(b) and (c)).

	Region *a*		Region *b*	
	As deposited	Annealed	As deposited	Annealed
σ_{22}	−15.7	−1.6	−9.8	−1.1
σ_{33}	−30.6	−3.1	−28.5	−2.9
σ_{zz}	−6.1	−0.6	−1.3	−0.1
σ_{rz}	−8.2	−0.8	−2.8	−0.3

As the observed corrosion damage extended along the interface between the different layers, it is necessary now to consider the driving force responsible for interfacial cracks observed at the corner of the micron-scale defects (Figs. 2(a) and 3(c), (d))? Interfacial cracks are known to appear when the shear stress or tensile stress exceeds the bonding strength of the interface. Therefore, it is more convenient to represent the residual stress in terms of normal (σ_{zz}) and shear (σ_{rz}) components within a polar coordinate system, the *r*-direction of which is parallel to the interfaces in the following discussion. The distributions of compressive stress normal to the TiSiN/TiN interface, σ_{zz}, and shear stress along the interface, σ_{rz}, are shown for the as-deposited sample in Fig. 5(b) and (c). The maximum shear stress of the as-deposited sample is ~9 times larger than that in the annealed sample, at both regions *a* and *b* (Table 2). Note that in a defect-free coating/substrate system the shear stress along the interface should be zero, which has been confirmed by our modeling results. The cross-sectional observation of the

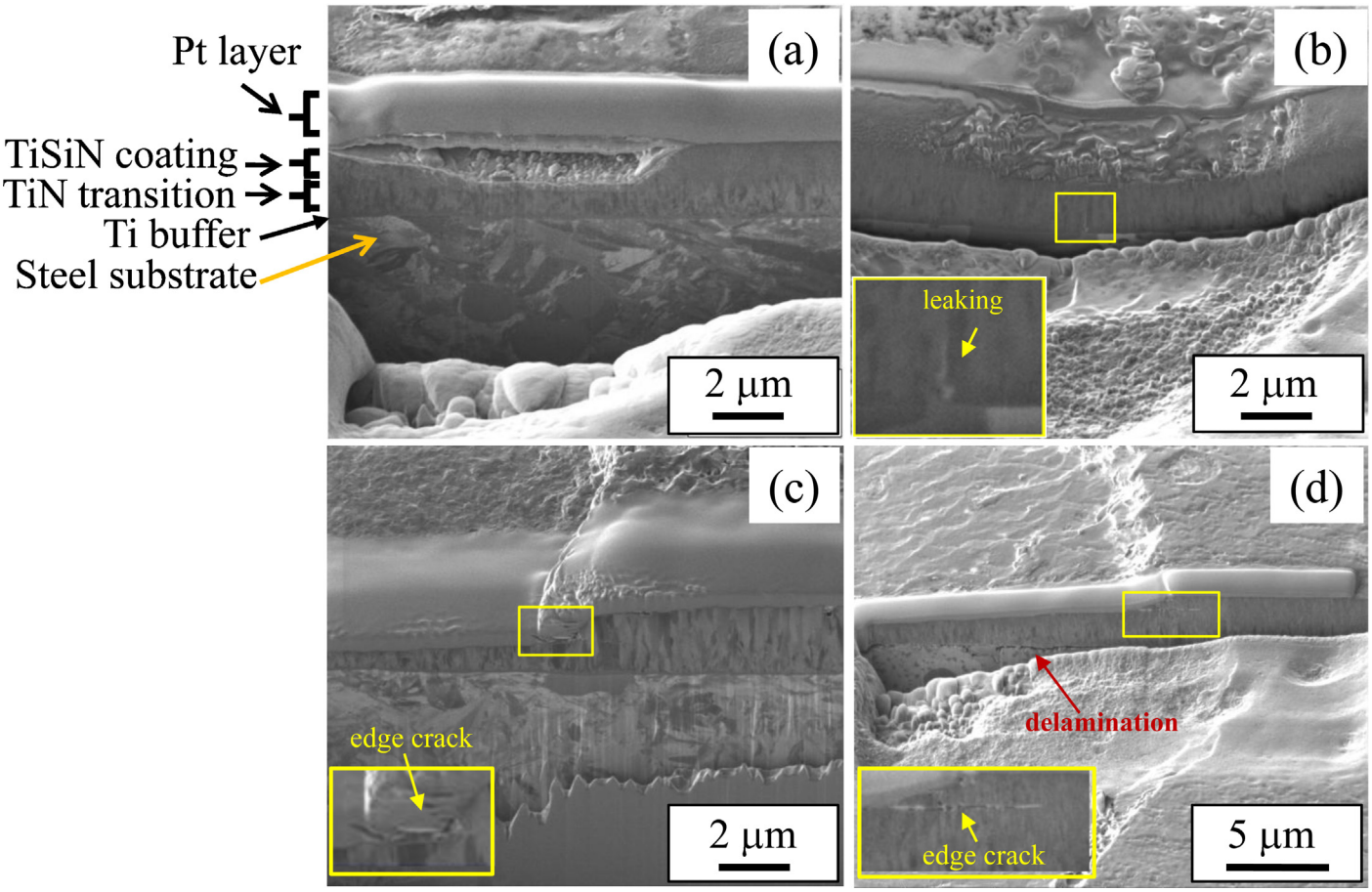

Fig. 3. Focused ion beam (FIB) generated cross-sectional micrographs of corrosion-induced damage in a cavity in (a) as-deposited [30] and (b) annealed sample after the 2 days corrosion test [30], (c) as-deposited and (d) annealed sample after the 8-day immersion test. Note that in (b) the corrosive agent penetrated through an intercolumnar fissure within the TiN layer which has partly closed up from the top, whereas in (d) the upper crack (i.e., the edge crack) appears to propagate along the TiSiN and TiN boundary and the lower crack (i.e., delamination) also extends along the coating and steel interface. In (a) Pt layer was deposited inside the FIB chamber before milling/sectioning. It protects the region of interest from the potential damage caused by FIB milling.

surface defects in the coating samples before corrosion showed no crack or delamination occurring at the corner of the pore (Fig. 2(c)), indicating that their bonding strength was higher than the maximum shear stress. However, the interfacial bonding may become weakened at the surface region, due to exposure to the acid. This explains why the edge cracks occurred at the TiSiN/TiN interface in the as-deposited sample, apparently driven by a high shear stress. At the same time, the maximum compressive stress within the as-deposited sample is also larger (~9 times) than that in the annealed sample in both regions. High compressive stress is understood to reduce the propagation of the interfacial cracks, and hence enhance the corrosion resistance of the as-deposited sample. Consequently, more severe delamination was observed in the annealed sample, as seen in Fig. 3(c) and (d).

3.3. *FEA modeling of nano-sized defects*

While the micron-scale surface defects are often involved in pitting (Fig. 2), it is much smaller, pre-existing coating defects that exhibit dimensions typically at a nanometer scale, such as pin-holes, cracks and intercolumnar fissures that play a governing role in corrosion development by acting as pathways for the penetration of corrosion agents to the less-noble steel substrate [12,13]. This is particularly true for the TiN coating layer in the current study (Fig. 3), which is known to have a columnar structure [33]. Moreover, because the dimensions of these defects are generally shorter than the wavelengths of the visible range, optically they could only be observed indirectly when an obvious corrosion trace presented (Fig. 3(b)).

In order to clarify the influence of localized residual stress upon the geometrical configuration of nano-scale defects in the TiN layer, two types of structural defects, namely, pin-holes and long fissures, were simulated. The diameter (or the width) of the defects was set to 30 nm, and the planar residual stresses applied were 3 GPa and 0.3 GPa, for the as-deposited and annealed samples, respectively. Our FEA simulation results showed that for the as-deposited samples the maximum shrinkage of the defect was less than 1% of the radius in the case of the pin-hole type defect, which is insignificant (Fig. 6(a)), and this also remained almost constant with respect to depth. In contrast, for long fissure type cracks, the maximum shrinkage of ~100% of the width was observed at the upper part of the TiN layer, suggesting that complete closure of the defect might occur at the top of the pin-hole (Figs. 6(b) and 7(a)). However, for the annealed samples, the maximum shrinkage was only ~10% for the same fissure due to a considerably lower residual stress being present in the coating (Fig. 6(c)). This helps explain the observation of corrosion damage in Fig. 3(b), where a fissure-type defect in the TiN layer was observed, acting as a passage for the corrosion agent, resulting in corrosion in the steel substrate, as illustrated in Fig. 7(b). After the 8-day corrosion test more severe corrosion at the TiN–steel substrate interface can be seen in the annealed sample (Fig. 3(d)), compared to the as-deposited sample (Fig. 3(c)), which

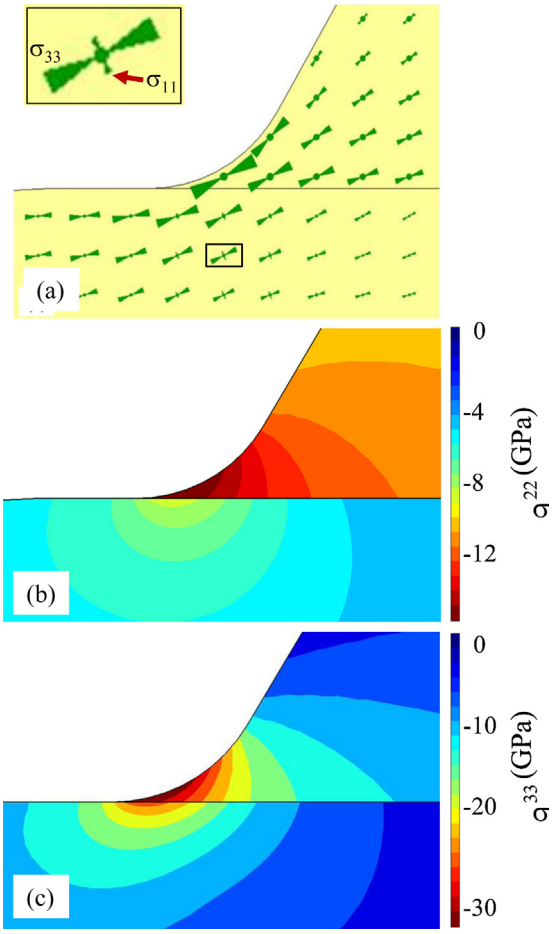

Fig. 4. Residual stress re-distribution around a micron-scale defect in region '*a*' (Fig. 1(b)) in the as-deposited sample simulated by finite element analysis (FEA): (a) three principal stresses. The directions of the principal axes are indicated by arrows, and magnitudes of the components are indicated by the size of the arrows. σ_{11} is within the image plane and vanishes at the surface, σ_{22} is perpendicular to the image plan, and σ_{33} is in plane, compressive and more evident near the surface. (b) Second principal stress, σ_{22}, which is normal to the viewing plane. The negative sign in the color scale indicates that the stress is predominantly compressive. (c) Third principal stress, σ_{33}, which is in plane and compressive.

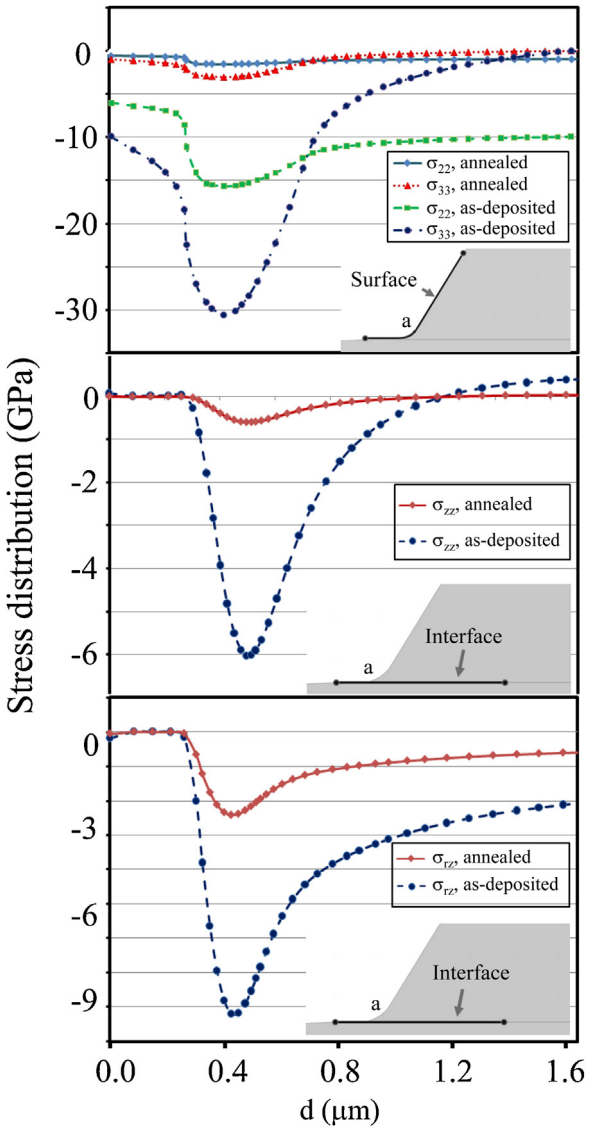

Fig. 5. Finite element analysis (FEA) results of residual stress distribution along the cavity surface and interface in region '*a*' of a micron-scale defect (as seen in Fig. 1(b)). The insets show the model geometries. The stress distribution is displayed along the bold lines within the models starting from the left. (a) Second and third principal stresses. (b) Normal compressive stress along the interface. (c) Shear stress along the interface. The horizontal scale, d, represents the distance along the bold lines.

supports the above finding. Obviously, this was a direct result from penetration of the corrosion agent through the TiN layer, although in this case no leakage pathway was directly observed. Notably, the partial closure of the defect at the top (Fig. 3(b)) may result from a downward bending of the coating layer caused by corrosion in the steel substrate. Furthermore, for a fissure type defect the shrinkage would increase rapidly from the bottom of the TiN layer in the presence of residual stress (Fig. 6(c)), indicating that the shrinkage would increase when the coating layer becomes thicker or the width of the fissure becomes narrower.

3.4. Conditions for closure of the fissures

The geometrical configuration of the fissure-type defects is critical when assessing the effect of compressive residual stress upon corrosion resistance. Normally this type of defect has a length much larger than its width, which satisfies the requirement of 2D plane strain symmetry used in our modeling. As such, the aspect ratio of the fissure defects, defined as the ratio of (coating thickness)/(width of the fissure), becomes a crucial factor (see Fig. 8(a)). The thickness of the TiN coating layer is typically 1–5 μm, while the width of the fissure through the coating is typically in the order of ~50 nm. As such, the defects usually have an aspect ratio of 20 to 100. A parametric scan of FEA models was performed to assess the impact of aspect ratio, in which a substrate with larger dimensions were adapted (100 μm × 100 μm) so as to keep the maximum coating thickness below 10% of that of the substrate, in order to minimize the effect of substrate bending. As seen from Fig. 8(b), which was obtained from the FEA parametric scan, for narrow fissures the coating thickness which is required to completely close the defect from the top increases almost linearly with the width of the fissure, meaning that the aspect ratio for any particular stress level is a constant. Hence, a key parameter, closure aspect ratio, can be defined for different stress levels. This parameter defines the threshold aspect ratio at which a top closure of the defect happens under specific stress levels. The larger the aspect ratio of a fissure, the greater the shrinkage of this defect would have under a compressive residual stress.

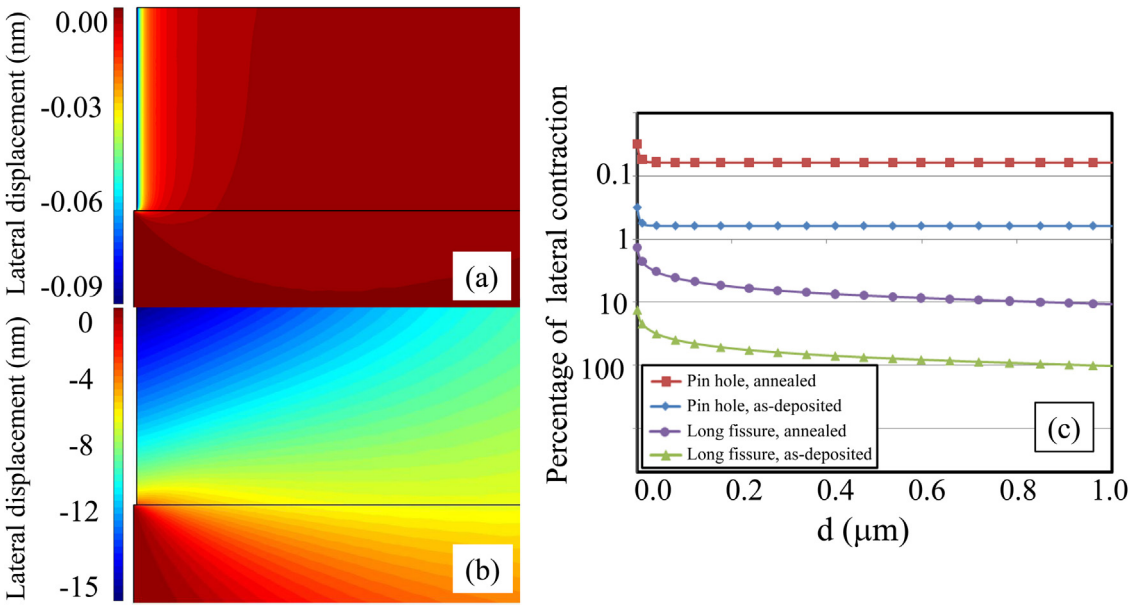

Fig. 6. Finite element analysis (FEA) results of the shrinkage behavior of nano-scale defects within the TiN coating layer of 1 μm thickness, induced by compressive residual stress. (a) Lateral contraction around a pin-hole of 15 nm in radius (Fig. 1(c) and (e)). (b) Lateral contraction across a fissure of 30 nm in width (Fig. 1(d) and (e)). (c) Percentage of lateral shrinkage for different types of coating defects, in a logarithmic scale, calculated along the wall of these defects. The horizontal axis, d, starts from the bottom of the defect moving upwards along the wall.

Notably, in this work the defects that act as the passage for the corrosion agent are within the TiN layer which exhibits a columnar structure (Fig. 3(b)) [33]. The through-thickness fissures are likely to coincide with intercolumnar grain boundaries, which are weaker than the columnar grains themselves. For the as-deposited sample with a residual stress of ~3 GPa, assuming the width of the fissures are below 30 nm, the coating thickness required to close up a fissure is ≤1 μm (see Fig. 8(b)). This is equivalent to the coating layer used in our experiments. On the other hand, the residual stress in the annealed sample is only 0.3 GPa that will leave the fissure completely open. Here, excellent agreement between the experimental results and the modeled prediction has been achieved. For the as-deposited coating, the resultant closure lowers the total cross-sectional area of the open defects, and in doing so, this closure effectively blocks the passage of the corrosive agent and limits the corrosion damage.

In general, in TiN coatings a residual stress greater than 3 GPa can close up fissures with a width of 100 nm, if the thickness of the coating is above 3 μm. A low residual stress (i.e., <1 GPa), however, is unable to close up fissures of the same size completely at this coating thickness (Fig. 8(b)). More complete closure of defects will require a higher residual stress or thicker coatings. Hence, it is possible to improve the coating corrosion resistance by adjusting the compressive residual stress in conjunction with the thickness of the coating, taking into account the typical dimensions of the defects which result from a particular deposition process. The closure aspect ratio plotted against residual stress is shown in Fig. 8(c). It can be seen that in a TiN coating a residual stress above 3 GPa is desirable that yields a closure aspect ratio 30, in which case the required thickness of the coating layer can be reduced, compared to the coatings with a lower compressive stress. Fig. 8(c) also provides a means to derive the coating thickness required for closing all the defects: for example, for ceramic coatings with typical fissures ~50 nm in width, 1 GPa compressive residual stress gives a closure aspect ratio of 100 that can be translated to a minimum coating thickness of 5 μm. It should be noted that for different coating materials, the required closure aspect ratios may also be evaluated numerically using similar FEA analysis.

Compared to a previous study [30], the modeling and analysis presented here provide a more conclusive explanation to the

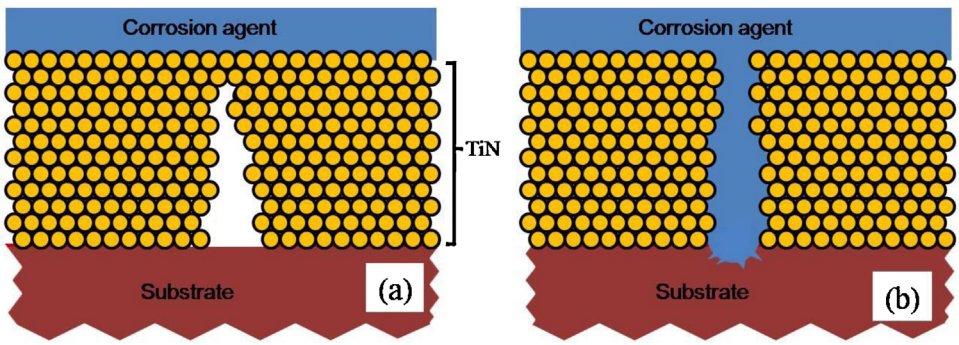

Fig. 7. Cross-sectional schematic diagrams of the fissure-type defects within the TiN layer under corrosive agent attack. (a) The closure of the upper part of the defect in the TiN layer induced by high residual stress within the TiN (as-deposited sample). (b) The surface defect remains open in the presence of low compressive residual stress within the TiN (annealed sample), consequently, the corrosion agent penetrates through the TiN layer, resulting in damage to the substrate. Note, the schematic diagrams are not to scale.

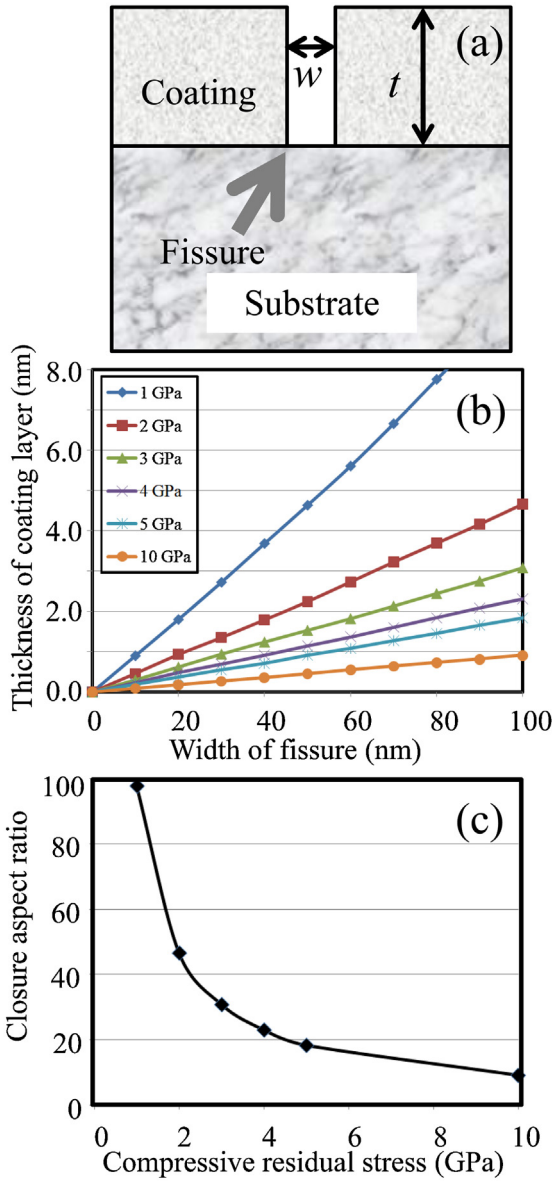

Fig. 8. (a) A cross-sectional view of a fissure-type defect in the coating layer. Aspect ratio = t/w. (b) The curves dedicate a seamless closure at the top of a fissure within the TiN coating layer having certain thickness under differing compressive residual stresses. The horizontal coordinate represents the width of the fissure, and the vertical coordinate represents the thickness of the coating layer. Different lines correspond to various level of compressive residual stress, as indicated by the templates in the inset. The linear relationship indicates that the 'closure aspect ratio is a constant for each stress level'. (c) The closure aspect ratio in the TiN coating, plotted as a function of the residual stress within the coating layer.

mechanisms that underlie the corrosion resistance of coating layers. It shows that the weakening of an interface due to a direct contact with a corrosive agent and the exposure of the substrate through pre-existing defects, instead of an ineffective acid attack to the coating layer itself, plays a dominant role in inflicting corrosion damage to a nanocomposite coated steel. More significantly, the modeling results and experimental observations showed excellent agreement, and a numerical relationship between the closure of the defects and its overarching parameters, i.e., residual stress, coating thickness and defect width, has been established, which may further assist in optimizing the corrosion resistant of nanocomposite coatings.

It is worth noting that, in a previous study, heat treatment was found to be highly effective for suppressing the preferential corrosion at the boundary of coating and substrate through diffusion process and sintering of micro-gaps [34]. Hence in this work, it is expected that some diffusion took place between the layers in the coating as well as between the bottom layer of Ti and the steel substrate during annealing. Sintering of some fine cracks may also be expected during annealing at 900 °C. This raises an intriguing question: why the corrosion resistance of the coated steel was reduced following annealing? The answer may lie in the change of residual stress observed in this work. According to our modeling results, a marked reduction in compressive stress in the coating, induced by the annealing, promotes the propagation of cracks (originating from the structural defects) both inside the coating and along the coating/substrate interface. As such, it would offset the beneficial effects of diffusion to a point that the overall corrosion resistance of coated steel declines, as observed in this work. On the basis of this understanding, it is suggested that during annealing two opposite trends affecting corrosion resistance of the coated steel, apparently caused by the diffusion and residual stress relief, may coexist and should be taken into account, when evaluating the performance of coated specimens against corrosive attack. Caution needs to be taken when applying heat treatment to improve the corrosion resistance of coated steel.

4. Conclusions

Nanocomposite coatings comprising an outer TiSiN layer and a columnar-structured TiN transitional layer were prepared. The mechanism through which compressive residual stress regulates the corrosion resistance of the coating layers was investigated by combining site-specific subsurface observation with FEA. The FEA results agree well with the experiment observations. The key findings can be summarized as follows:

1. Two different processes that underlie pitting were observed experimentally in the coatings: (a) cracks initiating at the corner of pre-existing micron-scale defects and propagating along the interface, driven by the combined effect of localized shear stress and corrosion-induced weakening, (b) delamination along the interface between the columnar-structured TiN and the substrate, resulting from the penetration of corrosion agent through nano-scale pin-holes and fissures.
2. At the surface of the micron-scale defects, the tangential compressive stress (σ_{22} and σ_{33}) improved the corrosion resistance of the as-deposited coating. Delamination occurred at the interface between the TiSiN and TiN coating layers around the corners of the micro-sized defects, apparently driven by the shear component of residual stress. However, its propagation was resisted by the compressive stress component which is normal to the interfaces. Both the shear and normal components were proportional to the compressive residual stress in the coatings.
3. The shrinkage, or closure, of nano-scale defects, facilitated by the compressive residual stress, is one of the key mechanisms through which the corrosion resistance of the coating system is enhanced.
4. Greater residual stress and a larger coating thickness will aid in the closure of through-coating defects and improve resistance to corrosion attack. The closure aspect ratio of the fissure-type defects is proposed as the key indicator that defines the corrosion resistance of coating layers dominated by this type of defect. Numerical results are obtained for closure aspect ratio in the TiN coating, as a function of defect width, coating thickness and residual stress.

5. Considering the beneficial effects of compressive stress in resisting the interfacial cracking, caution should be exercised when heat treatment is used to promote the diffusion effects.

A high residual stress in a thicker coating layer is particularly effective in enhancing the corrosion resistance of a coating layer with typical fissure-type defects, for example, in a columnar structured coating. The findings are expected to be used as a guide in designing and optimizing corrosion resistant coatings.

Conflict of interest

None declared.

Acknowledgements

The coating deposition and annealing were carried out by Dr ZF Zhou at the Advanced Coatings Applied Research Laboratory of the City University of Hong Kong. The immersion test was conducted with the assistance of Mr MS Ahmed at Edith Cowan University (ECU). Dr ZH Xie acknowledges the financial support provided by ECU through the Faculty Research Grant and the ECU-Industry Collaboration Scheme.

References

[1] A. Stierle, Science, 321, 349–350 (2008).
[2] T. Sidhu, S. Prakash and R. Agrawal, Acta Mater., 54, 773–784 (2006).
[3] P.H. Mayrhofer, C. Mitterer, L. Hultman and H. Clemens, Prog. Mater. Sci., 51, 1032–1114 (2006).
[4] C. Sun, R. Hui, W. Qu and S. Yick, Corros. Sci., 51, 2508–2523 (2009).
[5] Y. Li, L. Qu and F. Wang, Corros. Sci., 45, 1367–1381 (2003).
[6] S. Korablov, M.A.M. Ibrahim and M. Yoshimura, Corros. Sci., 47, 1839–1854 (2005).
[7] C. Liu, Q. Bi, A. Leyland and A. Matthews, Corros. Sci., 45, 1243–1256 (2003).
[8] X. Ding, A. Tan, X. Zeng, C. Wang, T. Yue and C. Sun, Thin Solid Films, 516, 5716–5720 (2008).
[9] Y. Yoo, D. Le, J. Kim, S. Kim and P. Vinh, Thin Solid Films, 516, 3544–3548 (2008).
[10] Q. Yang, F. Cai, L.R. Zhao and X. Huang, Surf. Coat. Technol., 203, 606–609 (2008).
[11] S.G. Harris, E.D. Doyle, Y.-C. Wonga, P.R. Munroe, J.M. Cairney and J.M. Long, Surf. Coat. Technol., 183, 283–294 (2004).
[12] P.M. Perillo, Corrosion, 62, 182–185 (2006).
[13] B. Subramanian, K. Ashok, K. Subramanian, D. Sastikumar, G. Selvan and M. Jayachandran, Surf. Eng., 25, 490–495 (2009).
[14] M. Kaufman and J. Fink, Acta Metall., 36, 2213–2228 (1988).
[15] T. Magnin, A. Chambreuil and B. Bayle, Acta Mater., 44, 1457–1470 (1996).
[16] T. Magnin, R. Chieragatti and R. Oltra, Acta Metall. Mater., 38, 1313–1319 (1990).
[17] K. Sieradzki and R. Newman, J. Phys. Chem. Solids, 48, 1101–1113 (1987).
[18] L. Xu and Y. Cheng, Corros. Sci., 59, 103–109 (2012).
[19] Y. Pauleau, Vacuum, 61, 175–181 (2001).
[20] L.B. Freund and S. Suresh, Thin Film Materials: Stress, Defect Formation, and Surface Evolution, Cambridge Univ. Press, Cambridge (2003).
[21] A. Cavaleiro, A.P. Marques, J.V. Fernandes, N.J.M. Carvalho and J.T. De Hosson, J. Mater. Res., 20, 1356–1368 (2005).
[22] J. Cheng, E. Jordan, B. Barber and M. Gell, Acta Mater., 46, 5839–5850 (1998).
[23] G. Knuyt, W. Lauwerens and L. Stals, Thin Solid Films, 370, 232–237 (2000).
[24] J. Swadener, B. Taljat and G. Pharr, J. Mater. Res., 16, 2091–2102 (2001).
[25] M. Bielawski, Surf. Coat. Technol., 200, 3987–3995 (2006).
[26] P. Kadolkar, T. Watkins, J. De Hosson, B. Kooi and N. Dahotre, Acta Mater., 55, 1203–1214 (2007).
[27] P.C. Wo, P.R. Munroe, M. Vasiliev, Z.H. Xie, K. Alameh and V. Kotov, Opt. Mater., 32, 315–322 (2009).
[28] Z.H. Xie, M. Hoffman, R.J. Moon and P.R. Munroe, J. Mater. Res., 21, 437–447 (2006).
[29] M.S. Ahmed, X. Zhao, Z. Zhou, P. Munroe, N. Chen-Tan, L.K.Y. Li and Z. Xie, J. Am. Ceram. Soc., 94, 1546–1551 (2011).
[30] M.S. Ahmed, P. Munroe, Z.T. Jiang, X. Zhao, W. Rickard, Z. Zhou, L.K.Y. Li and Z. Xie, Corros. Sci., 53, 3678–3687 (2011).
[31] E. Bemporad, M. Sebastiani, C. Pecchio and S. De Rossi, Surf. Coat. Technol., 201, 2155–2165 (2006).
[32] S. Ningshen and U.K. Mudali, Metallic and Oxide Coatings for Corrosion Protection in Corrosion Science and Technology: Mechanism, Mitigation and Monitoring, Ed. by U.K. Mudali and B. Raj, Alpha Science Intl Ltd, NY (2008).
[33] V. Jayaram, S. Bhowmick, Z. Xie, S. Math, M. Hoffman and S. Biswas, Mater. Sci. Eng. A, 423, 8–13 (2006).
[34] S. Kuroda, J. Kawakita, T. Fukushima and S. Tobe, Mater. Trans., 44, 381–388 (2003).